Journal of
Nanoscience and Nanotechnology
Vol. 7, 1753–1759, 2007

Double-Walled Carbon Nanotubes Under Hydrostatic Pressure: Raman Experiments and Simulations

Vikram Gadagkar[1], Surajit Saha[1,*], D. V. S. Muthu[1], Prabal K. Maiti[2], Yves Lansac[3], A. Jagota[4], Alexander Moravsky[5], R. O. Loutfy[5], and A. K. Sood[1]

[1] Department of Physics, Indian Institute of Science, Bangalore 560012, India
[2] Centre for Condensed Matter Theory, Department of Physics, Indian Institute of Science, Bangalore 560012, India
[3] LEMA, UMR 6157 CNRS-CEA, Université François Rabelais, 37200 Tours, France
[4] Department of Chemical Engineering, Lehigh University, Bethlehem, Pennsylvania 18015, USA
[5] Materials and Electrochemical Research Corporation, Tucson, AZ, USA

We have used Raman spectroscopy to study the behavior of double-walled carbon nanotubes (DWNT) under hydrostatic pressure. We find that the rate of change of the tangential mode frequency with pressure is higher for the sample with traces of polymer compared to the pristine sample. We have performed classical molecular dynamics simulations to study the collapse of single (SWNT) and double-walled carbon nanotube bundles under hydrostatic pressure. The collapse pressure (p_c) was found to vary as $1/R^3$, where R is the SWNT radius or the DWNT effective radius. The bundles showed ~30% hysteresis and the hexagonally close packed lattice was completely restored on decompression. The p_c of a DWNT bundle was found to be close to the sum of its values for the inner and the outer tubes considered separately as SWNT bundles, demonstrating that the inner tube supports the outer tube and that the effective bending stiffness of DWNT, $D_{DWNT} \sim 2D_{SWNT}$.

Keywords: DWNT, High Pressure, Raman Spectroscopy, Molecular Dynamics.

RESEARCH ARTICLE

1. INTRODUCTION

Since their discovery, carbon nanotubes have been the subject of keen theoretical and experimental investigations owing to their fascinating structural, electronic, and mechanical properties.[1] Carbon nanotubes promise applications in such varied fields as nanoelectronics, actuators, sensors,[2] nanofluidics, hydrogen storage, and high-strength materials. The mechanical properties of carbon nanotubes naturally depend on the number of coaxial graphitic cylinders that go into their making. Significant advances have already been made in the understanding of single (SWNT) and multi-walled (MWNT) carbon nanotubes. More recently, double-walled carbon nanotubes (DWNT) have been observed and synthesized[3,4] by heating C_{60} peapods. The first selective (selectivity ~97%) and efficient synthesis of DWNT in a one-step direct chemical process was demonstrated by Hutchison et al.[5] Being the simplest of the MWNT, with just two concentric cylinders, DWNT are ideal systems to study the evolution of various properties from the single to the multi-walled regime.

Hydrostatic as well as non-hydrostatic high-pressure experiments on SWNT have uncovered several remarkable features. Raman scattering and X-ray diffraction studies have been used to study the pressure dependence of the radial breathing mode (RBM) and translational order of the triangular lattice.[6] Under hydrostatic pressure, the RBM vanishes at ~2 GPa and recovers reversibly when decompressed from ~5 GPa but some workers find that it fails to do so when decompressed from a higher pressure.[7–9] However, Teredesai et al.[10] report the reappearance of the RBM even when decompressed from ~26 GPa. The current understanding is that nanotubes get distorted from their originally circular shape to an oval shape under pressure leading to a loss in the Raman resonance condition, the consequence of which is the loss in RBM intensity. The pressure coefficient of the tangential mode also changes slope at ~2 GPa, a phenomenon attributed to the flattening or polygonization of the nanotubes. High pressure X-ray diffraction studies also indicate a loss of the triangular lattice symmetry, which reappears under decompression.[11] Molecular dynamics simulations suggest that SWNT bundles[12,13] as well as isolated tubes[14–16] collapse under hydrostatic pressure and that the collapse pressure varies as an inverse power law of the tube radius.

*Author to whom correspondence should be addressed.

1533-4880/2007/7/1753/007 doi:10.1166/jnn.2007.710

Like the SWNT, the DWNT are also found to form in a triangular lattice.[17] More recently, several workers[18–22] have used Raman spectroscopy to study bundles of DWNT under hydrostatic pressure. Arvanitidis et al.[19] have concluded that the outer tube acts as a protective shield for the inner tube and the inner tube mechanically supports the outer tube under high pressure conditions. Puech et al.[20] report that the pressure coefficient for the tangential mode from the external tube is the same as that for SWNT and that for the inner tube is 45% smaller. They also find that the phonon band of the outer tube broadens with the application of pressure while that of the inner tube remains constant. A third study[21] reports high pressure Raman studies of DWNT using alcohol and argon as the pressure transmitting media. In alcohol, they identify two distinct modes in the G band (splitting) up to 10 GPa and a structural distortion at 3 GPa. The high and low frequency modes are attributed to the outer and inner tubes, respectively. In argon, they observe a transition at 6 GPa which removes the splitting. Venkateswaran[22] studied the behavior of the RBM of the inner and outer tubes as a function of pressure. It is found that the $(1/\omega)d\omega/dp$ of the outer tube follows the $\omega_{\mathrm{RBM}}^{-2}$ dependence whereas the RBM of the inner tube behaves similar to that of an isolated SWNT.

In this paper, we describe our high pressure Raman experiments and a set of molecular dynamics simulations performed to investigate the behavior of DWNT under pressure, focusing on the response of the inner and the outer tubes.

2. MATERIALS AND METHODS

2.1. Experimental Details

High pressure Raman scattering experiments were done on a sample of DWNT, which was grown using high temperature chemical vapor deposition (CVD) and deposited on PARAFILM® "M." Electron microscopy images in Figures 1(a) and (b) illustrate the structure and bundling of the as-produced CVD DWNT used in this work. The tubes obtained under standard production conditions are about 2.2 nm in diameter on the average, with ~0.5 nm width of diameter distribution, as assessed by TEM. The as-produced material contains predominantly relatively thin DWNT bundles, comprising 5–15 tubes, and also some individual tubes (~20% of the number of bundles). Bundles were found to be about 25 nm long, by SEM measurements. The as-produced DWNT are more than 90 wt% pure in carbon, the rest 10% is represented by amorphous carbon and low volatile organic coating of the tube surface. The fraction of similar diameter SWNT contained in the as-produced DWNT material obtained under standard conditions does not exceed 3%. That is, the ratio of the number of DWNT to SWNT is >30. The as-produced DWNT also contains about 30 wt% of iron metal catalyst

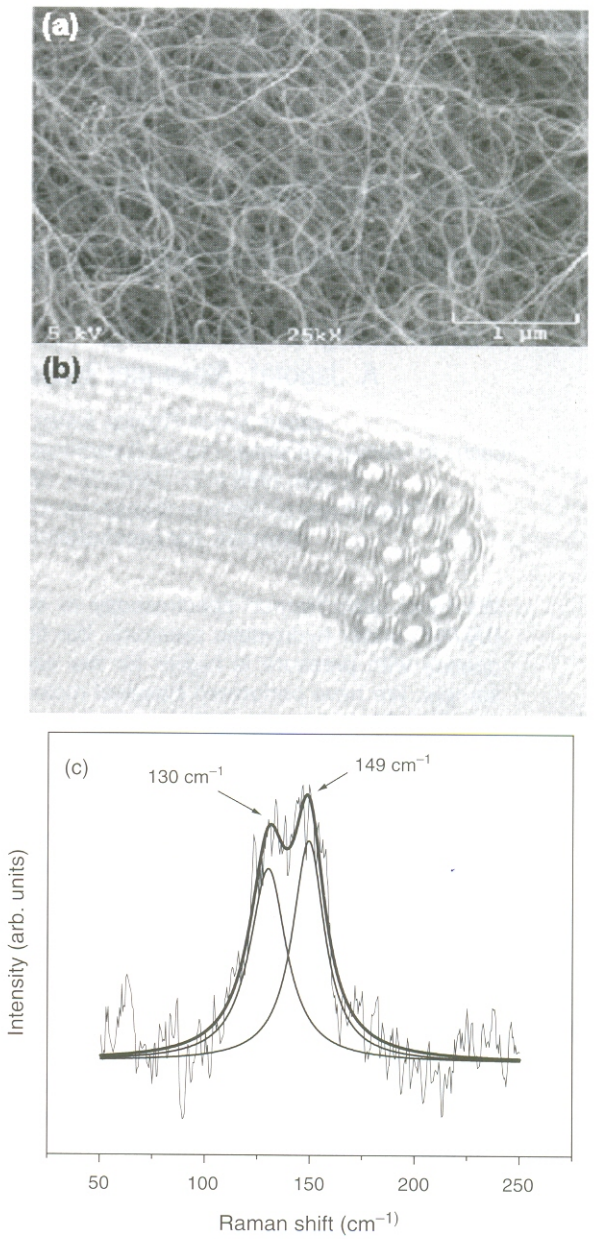

Fig. 1. High resolution SEM micrograph of as-produced CVD DWNT matted film used in the work (a), HRTEM Micrograph of a cross section of a CVD DWNT bundle, with individual tubes about 2.2 nm in diameter (b), and the radial breathing modes of the DWNT sample (c).

particles (by TGA), mainly encapsulated in thin carbon shells.

Raman spectra (Fig. 1(c)) show two radial breathing modes at 130 cm^{-1} and 149 cm^{-1}, which are expected for the outer tube diameter of ~2.2 nm as seen by electron microscopy. The nanotubes were separated from the PARAFILM® "M" by vigorously shaking the nanotube-coated film in chloroform. Once the sample was separated from the film, it was washed several times in chloroform to remove any part of the film that might be still sticking to the sample. This sample is referred to as the pristine DWNT sample. Experiments were also conducted on

Table I. Parameters for the C_R atom type (sp^2 hybridized carbon atom involved in resonance), in DREIDING,[24] a standard generic macromolecular force field used in all our molecular dynamics simulations.

$E_{\text{bond}}(R) = \frac{1}{2}K_b(R - R_0)^2$	$R_0 = 1.39$ Å	$K_b = 1050$ (kcal/mol)/Å^2	
$E_{\text{angle}}(\theta) = \frac{1}{2}K_\theta(\cos\theta - \cos\theta_0)^2$	$\theta_0 = 120°$	$K_\theta = 100$ (kcal/mol)/rad^2	
$E_{\text{torsion}}(\phi) = \frac{1}{2}V\{1 - \cos[n(\phi - \phi_0)]\}$	$\phi_0 = 180°$	$V = 25.0$ kcal/mol	$n = 2$
$E_{\text{inv}}(\Psi) = \frac{1}{2}\frac{K_i}{(\sin\Psi_0)^2}(\cos\Psi - \cos\Psi_0)^2$	$\Psi_0 = 0°$	$K_i = 40$ (kcal/mol)/rad^2	
$E_{\text{vdW}}(R) = D_0\left\{\left(\frac{R_0}{R}\right)^{12} - 2\left(\frac{R_0}{R}\right)^{6}\right\}$	$R_0 = 3.8983$ Å	$D_0 = 0.0951$ kcal/mol	

DWNT samples that were not washed once they were separated from the PARAFILM® "M." These are referred to as the DWNT-Polymer Composite (DPC) samples.

The high-pressure Raman experiments were done at room temperature in a gasketed Mao-Bell-type Diamond-Anvil Cell (DAC) with a mixture of methanol, ethanol, and water in the ratio 16:3:1 as the pressure transmitting medium. The ruby fluorescence technique[23] was used for the *in-situ* measurement of pressure. The sample was excited with an Ar^+ ion laser (Spectra Physics Model 165) lasing at 514.5 nm and the back-scattered light was analyzed using the SPEX Ramalog 5 spectrometer, a double grating monochromator with a cooled photomultiplier tube and a digital counter interfaced with a computer.

The behavior of the tangential modes was followed as a function of pressure from atmospheric pressure to about 13 GPa and back. The tangential modes were found to fit well to two Lorentzian curves. The radial modes of the DWNT could not be followed as a function of pressure owing to poor signal quality.

2.2. Simulation Methodology

We used DREIDING,[24] a standard generic macromolecular force field, in our molecular dynamics (MD) simulations. The force field parameters used to calculate intra and inter molecular interactions are listed in Table I. Previously, Elliott et al.[12] have successfully used this force field to study the collapse of SWNT bundles under hydrostatic pressure. We employed ModulaSim,[25] a modular and general purpose molecular modeling package to perform the simulations using the constant particle number, pressure, and temperature (NPT) ensemble. The Berendsen thermostat and barostat[26] were used to maintain the temperature (300 K) and the applied hydrostatic pressure. The simulation cell consisted of 16 independent SWNT or DWNT arranged in a hexagonally close packed 4×4 bundle, with periodic boundary conditions and pressure applied along all three mutually perpendicular directions. The tubes were all of the armchair type (n, n) and ten unit cells long (2.3 nm). Elliott et al.[12] have shown that nine independent tubes, ten unit cells long, are sufficient to avoid finite size effects. We carried out the MD simulations on four SWNT bundles, (5, 5), (10, 10), (15, 15), and (20, 20) and four DWNT bundles, (5, 5)@(10, 10), (7, 7)@(12, 12), (10, 10)@(15, 15), and (15, 15)@(20, 20) using the standard velocity Verlet algorithm to integrate the equations of motion. The gap between the inner and the outer tubes is ~3.4 Å, close to the inter-layer gap in graphite. This is simply a consequence of the choice of the inner and the outer tubes to be (n, n) and $(n + 5, n + 5)$, respectively. The bundles were initially equilibrated at atmospheric pressure and subsequently subjected to step-wise monotonically increasing hydrostatic pressure increments, letting the unit cell volume equilibrate for a minimum of 10 ps at each step. The simulation time step was 1 fs. Information about the structural transitions was obtained by plotting the unit cell volume (after equilibration at each hydrostatic pressure step) as a function of pressure.

3. RESULTS AND DISCUSSION

3.1. Experiments

Figure 2(a) shows representative Raman spectra, along with the fits, of the pristine DWNT sample at four pressures during the increasing pressure cycle and one after return from the highest pressure of 13.0 GPa. It can be seen that the spectrum at 0.9 GPa in the decreasing pressure cycle resembles the spectrum recorded at 1.2 GPa during the increasing pressure cycle. This recovery on pressure release demonstrates the mechanical resilience of the DWNT sample. The variation of frequency (ω) versus pressure (p) for the two modes is plotted in Figure 2(b). The values of $d\omega/dp$ for the two modes are 8.5 ± 1.3 and 6.8 ± 0.5 cm^{-1}/GPa, respectively.

High pressure Raman spectra were also recorded for the DPC sample. The representative spectra along with the fits are shown in Figure 3(a). As for the pristine sample, we see that this sample also shows almost complete recovery on pressure release from 14 GPa. Figure 3(b) shows the variation of mode frequency as a function of pressure for the two modes. It is intriguing to observe that these modes show much higher $d\omega/dp$ values (13.2 ± 1.3 and

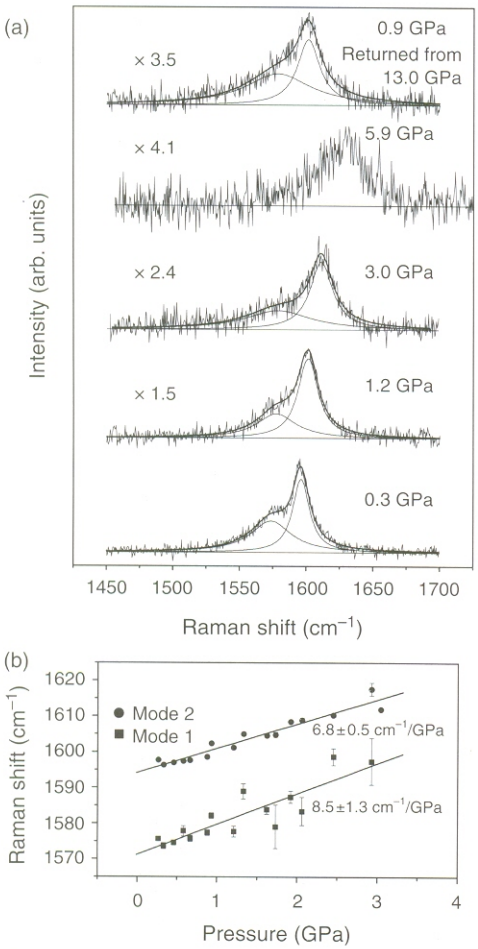

Fig. 2. A few representative tangential mode spectra of the pristine DWNT sample along with the two fit modes (a) and the variation of mode frequency as a function of pressure (b).

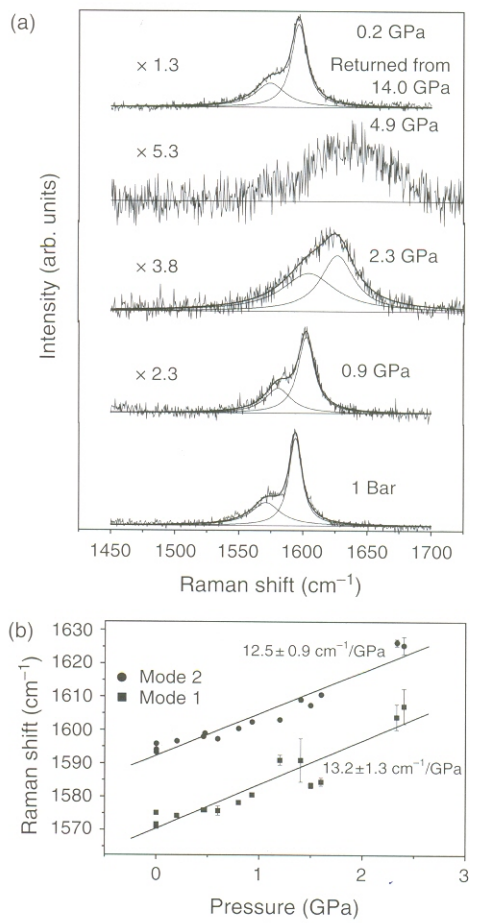

Fig. 3. A few representative tangential mode spectra of the DPC sample along with the two fit modes (a) and the variation of mode frequency as a function of pressure (b).

12.5 ± 0.9 cm^{-1}/GPa) than the corresponding modes of the pristine sample. We do not fully understand this result although the following observations can be made. The DWNT sample was originally deposited on a polymer film (PARAFILM® "M"). Shaking the DWNT coated film in chloroform separates the film and the nanotubes. It is possible, however, that some amount of the polymer still remains with the nanotubes. Washing the nanotubes repeatedly with chloroform probably has the effect of removing the remnants of polymer from the nanotubes. The much higher $d\omega/dp$ values for the DPC sample compared to the pristine DWNT sample seems to indicate that the presence of the polymer somehow increases the $d\omega/dp$ of the DWNT modes. The polymer present in the DPC sample may plug the ends of open tubes, thus preventing the transmitting medium from penetrating the tube and facilitating the tube deformation under external pressure. The polymer itself would slightly penetrate deep in the tube, however, and exert hydrostatic counteraction. In addition, the as-produced DWNT are coated with a thin organic layer (~5–7% of the tube weight by TGA) that consists presumably of high molecular weight alkyl aromatic molecules. The effect of this layer might be similar to that of the polymer from PARAFILM® "M." However, the layer can be at least partially removed by dissolution in some solvents such as chloroform. In this case its function to preserve the closed state of the end is lost, resulting in a lower $d\omega/dp$ values for the pristine sample. Clearly, more work needs to be done to resolve this issue, which will have some relevance to applications of nanotubes in super-tough polymer composites.

3.2. Simulations

The SWNT and DWNT equilibrated at atmospheric pressure have nearly circular cross sections, as shown in Figures 4(a), (c), and (e), and 5(a), (c), and (e) for SWNT and DWNT bundles, respectively. At atmospheric pressure, we find that $r_{min}/r_{max} \geq 0.93$ where r_{min} and r_{max} are the shortest and the longest distances from the center to the circumference of the tube cross section. It may be noted from Figure 5(b) that the $(7,7)@(12,12)$ is hexagonally faceted after the collapse pressure. To see the structural transition, we plot the reduced volume (V/V_0), where V_0 is the unit cell volume at atmospheric pressure, for the

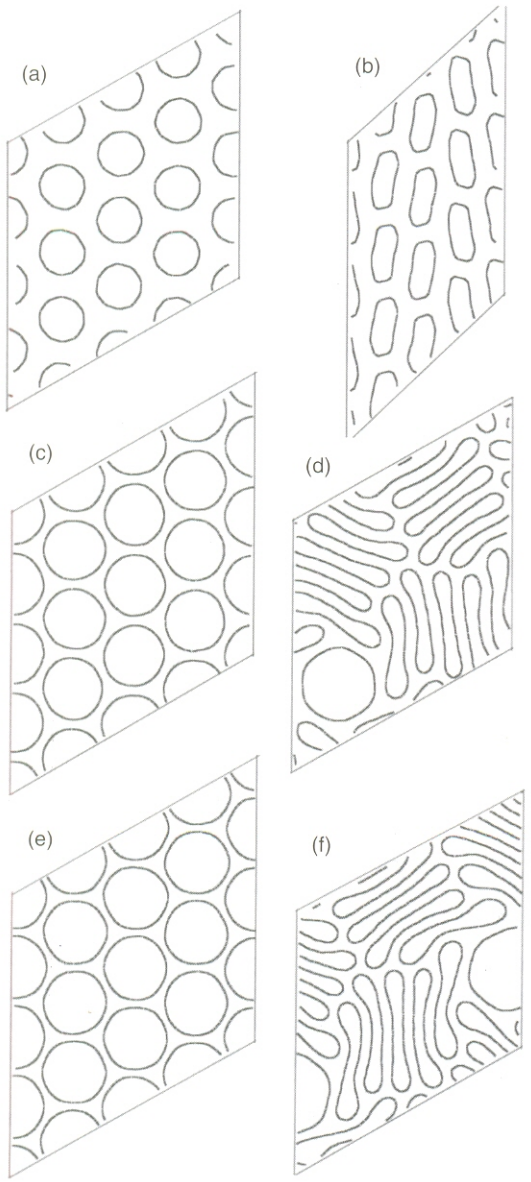

Fig. 4. Cross sections of three 4×4 SWNT bundles before and after collapse: $(5,5)$ at 1 atm before collapse (a) and 40 GPa after collapse (b), $(15,15)$ at 1 atm before collapse (c) and 2 GPa after collapse (d), and $(20,20)$ at 1 atm before collapse (e) and 1 GPa after collapse (f).

SWNT bundles as a function of pressure. Figure 6(a) shows these plots for three SWNT bundles. It is clear that all the SWNT bundles undergo a spontaneous structural transition at a critical pressure (p_c). Further, the critical pressure decreases with tube radius, in agreement with previously published results.[12, 13] Unless otherwise specified, p_c refers to the structural critical pressure on the loading curve. On plotting the reduced volume versus pressure for the DWNT bundles, as shown in Figure 6(b) for three bundles, we once again observe clear structural transitions at well-defined critical pressures. Till the critical pressure is reached, the tube cross sections remain almost circular

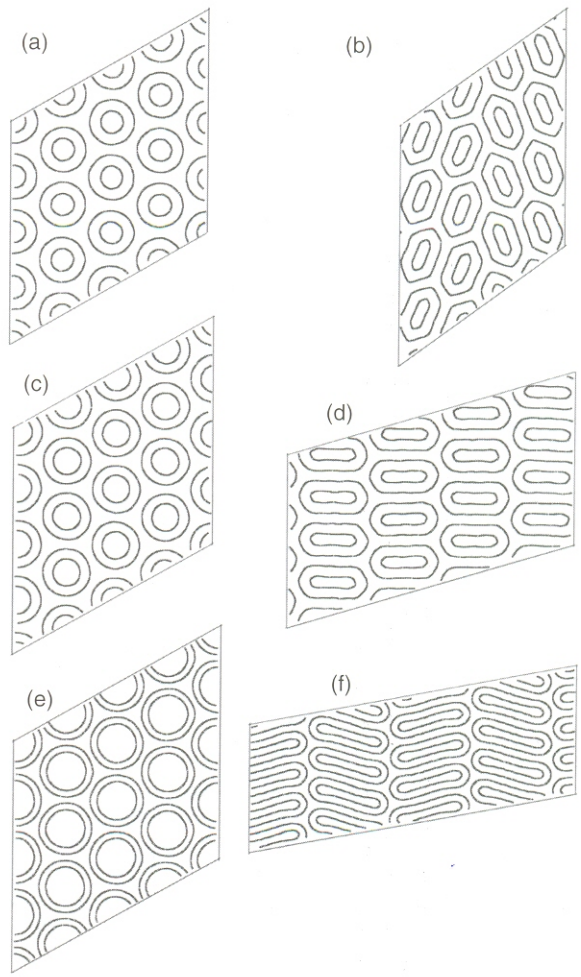

Fig. 5. Cross sections of three 4×4 DWNT bundles before and after collapse: $(5,5)@(10,10)$ at 1 atm before collapse (a) and 40 GPa after collapse (b), $(7,7)@(12,12)$ at 1 atm before collapse (c) and 20 GPa after collapse (d), and $(15,15)@(20,20)$ at 1 atm before collapse (e) and 4 GPa after collapse (f).

with slight deformations from the circular shape. When the applied hydrostatic pressure exceeds p_c, however, the tube cross sections become elliptical. Further increase in pressure results in a dumbbell shape as shown in Figures 4(b), (d), and (f), and 5(b), (d), and (f) for SWNT and DWNT bundles, respectively. The loading (pressure increase) and unloading (pressure decrease) curves show a $\sim$30% hysteresis in all the bundles studied. The hysteresis is calculated as $100\% \times [p_c^{\text{loading}} - p_c^{\text{unloading}}]/p_c^{\text{loading}}$. On decompression, we find that the hexagonally close packed lattice is completely restored in all the SWNT and DWNT bundles.

A closer look at the critical pressures of the DWNT bundles in Figure 6(b) reveals several remarkable features. First, we observe that the p_c of a given DWNT bundle is greater than the p_c of the SWNT bundle consisting of the corresponding outer tubes alone. For instance, the p_c of the $(15,15)@(20,20)$ DWNT is 1.4 GPa, which is higher as compared to the p_c of $(20,20)$ SWNT (0.3 GPa).

RESEARCH ARTICLE

4. SUMMARY

To summarize, DWNT bundles have been studied under pressure using Raman spectroscopy and molecular dynamics. The rate of change of the tangential mode frequency with pressure is higher for the DWNT with traces of polymer compared to the pristine DWNT. Using classical MD simulations, we show that DWNT bundles collapse at a critical pressure p_c that, like in the case of SWNT, varies as $1/R_{\text{eff}}^3$, where R_{eff} is a suitably defined effective radius. We find that the SWNT and DWNT bundles show complete recovery on decompression. The simulations clearly show that the inner tube supports the outer tube and enhances the stability of the DWNT under pressure.

Acknowledgments: A. K. S. thanks the Department of Science and Technology, Government of India, for financial support. V. G. thanks KVPY, Government of India, for financial support.

References and Notes

1. R. Saito, G. Dresselhaus, and M. S. Dresselhaus, Physical Properties of Carbon Nanotubes, Imperial College Press, London (**1998**).
2. S. Ghosh, A. K. Sood, and N. Kumar, *Science* 299, 1042 (**2003**).
3. B. W. Smith, M. Monthioux, and D. E. Luzzi, *Nature (London)* 396, 323 (**1998**).
4. S. Bandow, M. Takizawa, K. Hirahara, and M. Yudasaka, *Chem. Phys. Lett.* 337, 48 (**2001**).
5. J. L. Hutchison, N. A. Kiselev, E. P. Krinichnaya, A. V. Krestinin, R. O. Loutfy, A. P. Moravsky, V. E. Muradyan, E. D. Obraztsova, J. Sloan, S. V. Terekhov, and D. N. Zakharov, *Carbon* 39, 761 (**2001**); A. P. Moravsky, E. M. Wexler, and R. O. Loutfy, Carbon Nanotubes Science and Applications, edited by M. Meyyappan, CRC Press, Boca Raton (**2005**), Ch. 3, p. 65.
6. A. K. Sood, *Radiation Physics and Chemistry* 70, 647 (**2004**).
7. U. D. Venkateswaran, A. M. Rao, E. Richter, M. Menon, A. Rinzler, R. E. Smalley, and P. C. Eklund, *Phys. Rev. B* 59, 10928 (**1999**).
8. M. J. Peters, L. E. McNeil, J. P. Lu, and D. Kahn, *Phys. Rev. B* 61, 5939 (**2000**).
9. J. Sandler, M. S. P. Shaffer, A. H. Windle, and M. P. Halsall, *Phys. Rev. B* 67, 035417 (**2003**).
10. P. V. Teredesai, A. K. Sood, D. V. S. Muthu, R. Sen, A. Govindaraj, and C. N. R. Rao, *Chem. Phys. Lett.* 319, 296 (**2000**).
11. S. M. Sharma, S. Karmakar, S. K. Sikka, P. V. Teredesai, A. K. Sood, A. Govindaraj, and C. N. R. Rao, *Phys. Rev. B* 63, 205417 (**2001**).
12. J. A. Elliott, J. K. W. Sandler, A. H. Windle, R. J. Young, and M. S. P. Shaffer, *Phys. Rev. Lett.* 92, 095501 (**2004**).
13. X. H. Zhang, D. Y. Sun, Z. F. Liu, and X. G. Gong, *Phys. Rev. B* 70, 035422 (**2004**).
14. R. B. Capaz, C. D. Spataru, P. Tangney, M. L. Cohen, and S. G. Louie, *Phys. Stat. Sol. (b)* 241, 3352 (**2004**).
15. D. Y. Sun, D. J. Shu, M. Ji, Feng Liu, M. Wang, and X. G. Gong, *Phys. Rev. B* 70, 165417 (**2004**).
16. P. Tangney, R. B. Capaz, C. D. Spataru, M. L. Cohen, and S. G. Louie, *Nano Lett.* 5, 2268 (**2005**).
17. W. Ren, F. Li, J. Chen, S. Bai, and H.-M. Cheng, *Chem. Phys. Lett.* 359, 196 (**2002**).
18. R. Pfeiffer, H. Kuzmany, Ch. Kramberger, Ch. Schaman, T. Pichler, H. Kataura, Y. Achiba, J. Kürti, and V. Zólyomi, *Phys. Rev. Lett.* 90, 225501 (**2005**).
19. J. Arvanitidis, D. Christofilos, K. Papagelis, K. S. Andrikopoulos, T. Takenobu, Y. Iwasa, H. Kataura, S. Ves, and G. A. Kourouklis, *Phys. Rev. B* 71, 125404 (**2005**).
20. P. Puech, H. Hubel, D. J. Dunstan, R. R. Bacsa, C. Laurent, and W. S. Bacsa, *Phys. Rev. Lett.* 93, 095506 (**2004**).
21. P. Puech, H. Hubel, D. J. Dunstan, A. Bassil, R. Bacsa, A. Peigney, and E. Flahaut, *Phys. Stat. Sol. (b)* 241, 3360 (**2004**).
22. U. D. Venkateswaran, *Phys. Stat. Sol. (b)* 241, 3345 (**2004**).
23. R. A. Foreman, G. J. Piermarini, J. D. Barnet, and S. Block, *Science* 176, 284 (**1972**).
24. S. L. Mayo, B. D. Olafson, and W. A. Goddard III, *J. Phys. Chem.* 94, 8897 (**1990**).
25. ModulaSim was originally developed at the Material and Process Simulation Center, California Institute of Technology, CA, USA. http://ruby.wag.caltech.edu/Projects/ModulaSim/index.html. It is now actively being developed at the University of Tours (YL), IISc, Bangalore (PKM), and University of Colorado, Boulder (Matthew A. Glaser).
26. H. J. C. Berendsen, J. P. M. Postma, W. F. van Gunsteren, A. DiNola, and J. R. Haak, *J. Chem. Phys.* 81, 3684 (**1984**).
27. S. Timoshenko and S. Woinowsky-Krieger, Theory of Plates and Shells, 2nd edn., McGraw-Hill, New York (**1959**).
28. R. Frisch-Fay, Flexible Bars, Butterworths, Washington, DC (**1962**).
29. V. Gadagkar, P. K. Maiti, Y. Lansac, A. Jagota, and A. K. Sood, *Phys. Rev. B* 73, 085402 (**2006**).
30. X. Ye, D. Y. Sun, and X. G. Gong, *Phys. Rev. B* 72, 035454 (**2005**).
31. B. Yakobson, C. Brabec, and J. Bernholc, *Phys. Rev. Lett.* 76, 2511 (**1996**).
32. A. Pantano, D. M. Parkes, and M. C. Boyce, *J. Mech. Phys. Solids* 52, 789 (**2004**).
33. T. Tang, A. Jagota, and C.-Y. Hui, *J. Appl. Phys.* 97, 074304 (**2005**).
34. T. Tang, A. Jagota, C.-Y. Hui, and N. J. Glassmaker, *J. Appl. Phys.* 97, 074310 (**2005**).

Received: 30 April 2006. Accepted: 21 August 2006.